Organic Electronics 38 (2016) 172–179

Contents lists available at ScienceDirect

Organic Electronics

journal homepage: www.elsevier.com/locate/orgel

Letter

Oligothiophene-based small molecules with 3,3′-difluoro-2,2′-bithiophene central unit for solution-processed organic solar cells

Bin Kan [a, b], Qian Zhang [a, b], Xiangjian Wan [a, b, *], Xin Ke [a, b], Yunchuang Wang [a, b], Huanran Feng [a, b], Mingtao Zhang [a, b], Yongsheng Chen [a, b, *]

[a] State Key Laboratory and Institute of Elemento-Organic Chemistry, Collaborative Innovation Center of Chemical Science and Engineering (Tianjin), School of Materials Science and Engineering, Nankai University, Tianjin, 300071, China
[b] Key Laboratory of Functional Polymer Materials and the Centre of Nanoscale Science and Technology, Institute of Polymer Chemistry, College of Chemistry, Nankai University, Tianjin, 300071, China

ARTICLE INFO

Article history:
Received 25 June 2016
Received in revised form
31 July 2016
Accepted 11 August 2016

Keywords:
Organic solar cell
Small molecule
Oligothiophene
Fluorinated central unit

ABSTRACT

Two new oligothiophene-based small molecules, namely **DRCN6T-F** and **DRCN8T-F**, with 3,3′-difluoro-2,2′-bithiophene as the central building block and 2-(1,1-dicyanomethylene)-rhodanine as end groups, were designed and synthesized. Compared to their non-fluorinated counterparts **DRCN6T** and **DRCN8T**, **DRCN6T-F** and **DRCN8T-F** exhibit enhanced intermolecular interactions and lower HOMO energy levels. However, PCEs of 2.26% and 5.07% were obtained for **DRCN6T-F** and **DRCN8T-F** based optimized devices, respectively, lower than those of non-fluorinated molecules **DRCN6T** and **DRCN8T**. The relatively poor performance for the **DRCN6T-F** and **DRCN8T-F** were mainly caused by their low short-circuit current densities, due to their unfavorable morphologies and low charge carrier mobilities.

1. Introduction

Organic photovoltaic's (OPVs) with bulk heterojunction (BHJ) architectures are considered as a promising solar energy conversion technology possessing the advantages of solution-processablility, low-cost, flexibility and potential for large-area fabrication [1]. With much efforts, polymer-based and small/oligomer-molecule-based OPVs (SM-OPVs) have made an impressive progress with encouraging power conversion efficiencies (PCEs) surpassing the milestone of 10% [2–10]. These progress are attributed to the development of novel donor and acceptor materials, along with innovations and optimizations in device processing [11–18].Considering the advantages of small molecules, including their well-defined but versatile chemical structures, thus easier energy level control, and no batch to batch variations, small molecules are supposed to be good candidates for providing reliable analyses of chemical structure-properties-device performance relationships, which is of crucial importance for further molecular design with high performance [19–28].

Among various molecular designing strategies, the substitution of fluorine atom has attracted much attention in the past few years, and it has been demonstrated that fluorination is an effective method of tuning molecular energy levels, intramolecular and/or intermolecular interactions of conjugated polymers and small molecules, thus affecting their photovoltaic performance [29–35]. For example, Yan et al. reported a series of difluorinated benzo[c][1,2,5] thiadiazole (ffBT) based polymers with the best PCE of 11.7%, which is the highest result for the single junction organic solar cells so far [2,36]. Bazan's group designed and synthesized a D_1-A-D_2-A-D_1 type small molecule *p*-DTS(FBTTh$_2$)$_2$ with 5-fluorobenzo[c][1,2,5] thiadiazole (FBT) as acceptor units, which yielded a high PCE over 9% due to its desirable optical, electronic and physical properties [37]. Recently, other similar FBT based D_1-A-D_2-A-D_1 type small molecules with high performance were reported by Wang and Wu et al. [38,39]. While, in some cases, fluorination will lead to detrimental effects on performance, which has been partially explained by greater sensitivity to processing conditions due to their reduced solubility and poor compatibility with fullerene molecules, and greater tendency of fluorinated materials to aggregate [40–42]. For example, Yu et al. reported a series of fluorinated polymers, namely PTBF0, PTBF1, PTBF2 and PTBF3. Two

* Corresponding authors. State Key Laboratory and Institute of Elemento-Organic Chemistry, Collaborative Innovation Center of Chemical Science and Engineering (Tianjin), School of Materials Science and Engineering, Nankai University, Tianjin, 300071, China.

http://dx.doi.org/10.1016/j.orgel.2016.08.014
1566-1199/

fluorinated polymers (PTBF2 and PTBF3) exhibit poorer performance and lower mobilities than non-fluorinated polymer PTBF0. The lower mobilities for the fluorinated molecules are not unusual since factors (i.e., the molecular weight and polydispersity of the polymer, interconnection between neighboring phase, the domain boundary structure, and defects in the films) other than film crystallinity can influence the mobility [41]. In 2014, our group has also reported an acceptor-donor-acceptor (A-D-A) type small molecule with fluorinated end groups for solution-processed OPVs, and a relatively low PCE of 2.26% was obtained due to its poor morphology and low charge carrier mobility [43].

Recently, we have reported a series of oligothiophene-based A-D-A type small molecules, namely DRCN4T-DRCN9T, with 4–9 conjugated thiophene units as the molecule backbone, for solution processed OPV devices [6,44]. Here, in order to understand the impact of fluorinated central unit on the properties of oligothiophene-based A-D-A small molecules, we designed and synthesized two new oligothiophene-based small molecules, namely **DRCN6T-F** and **DRCN8T-F**, with 3,3′-difluoro-2,2′-bithiophene as the central building block. 2-(1,1-dicyanomethylene)-rhodanine was selected as the end groups and their specific chemical structures are depicted in Scheme 1. **DRCN6T-F** and **DRCN8T-F** possess similar chemical structures compared with **DRCN6T** and **DRCN8T** except for the replacement of C–H bond with C–F bond in the 2,2′-bithiophene unit. Their thermal stability, optical and electrochemical properties and photovoltaic performances were systematically investigated. PCEs of 2.26% and 5.07% were obtained for **DRCN6T-F** and **DRCN8T-F** based devices, respectively, lower than those of non-fluorinated molecules **DRCN6T** and **DRCN8T**. The relatively poor performance for the **DRCN6T-F** and **DRCN8T-F** were mainly caused by their low short-circuit current densities (J_{sc}s), due to their unfavorable morphologies and low charge carrier mobilities.

2. Experimental section

2.1. Materials and synthesis

All reactions and manipulations were carried out under argon atmosphere with the use of standard Schlenk techniques. All starting materials were purchased from commercial suppliers and used without further purification unless indicated otherwise. Compound 1, 3, 4 and 5 were synthesized according to the literature [44–46].

Compound 2. Under the protection of argon, *n*-butyllithium (2.4 M in hexane, 2.75 mL, 6.60 mmol) was dropwise added to the compound 1 (1.07 g, 3.00 mmol) in dry THF (20 mL) at −78 °C over 0.5 h. After stirring for 1 h, Bu_3SnCl (2.44 g, 7.50 mmol) was added into the mixture at −78 °C. Then the mixture was warmed to room temperature and stirred for 12 h. Subsequently, the mixture was poured into ice water and extracted with CH_2Cl_2 (50 mL × 2). The organic layer was washed with water and dried over anhydrous Na_2SO_4 for 3 h and concentrated to afford compound 4a, which was used for the next step without purification.

Compound DF6T-F. Under the protection of argon, compound 2 (1.50 mmol) and compound 3 (1.57 g, 3.15 mmol) in dry toluene (80 mL) were degassed for 15 min with argon following the addition of $Pd(PPh_3)_4$ (40 mg). After stirring and refluxing overnight, the reaction mixture was quenched with ice water (80 mL) and extracted with CH_2Cl_2 (100 mL × 2). The organic layer was washed with water and dried over anhydrous Na_2SO_4 over 2 h. After removal of solvent, the crude product was purified by silica gel using dichloromethane/petroleum (2:1) as eluent to give compound DF6T-F as a solid (0.95 g, 61%). ^{1}H NMR (400 MHz, $CDCl_3$): δ 9.84 (s, 2H), 7.60 (s, 2H), 7.13 (s, 2H), 6.95 (s, 2H), 2.84–2.78 (m, 8H), 1.71–1.68 (m, 8H), 1.41–1.25 (m, 32H), 0.88–0.86 (t, 12H); ^{13}C NMR (100 MHz, $CDCl_3$): δ 182.49, 154.59, 151.97, 141.26, 140.64, 140.38, 138.99, 133.62, 131.66, 130.50, 115.54, 115.28, 31.88, 30.45, 30.27, 29.49, 29.46, 29.41, 29.28, 22.70, 14.13. MS (MALDI-TOF) *m*/*z*: calcd for $C_{58}H_{76}F_2O_2S_6$ $[M]^+$, 1034.41; found, 1034.30.

Compound DF8T-F. Under the protection of argon, compound 2 (0.85 mmol) and compound 4 (1.24 g, 1.80 mmol) in dry toluene (80 mL) were degassed for 15 min with argon following the addition of $Pd(PPh_3)_4$ (30 mg). After stirring and refluxing overnight, the reaction mixture was quenched with ice water (80 mL) and extracted with CH_2Cl_2 (100 mL × 2). The organic layer was washed with water and dried over anhydrous Na_2SO_4 over 2 h. After removal of solvent, the crude product was purified by silica gel using dichloromethane/petroleum (1:1) as eluent to give compound DF8T-F as a solid (0.50 g, 42%).^{1}H NMR (400 MHz, $CDCl_3$): δ 9.83 (s, 2H), 7.59 (s, 2H), 7.12 (s, 2H), 7.01 (s, 2H), 6.93 (s, 2H), 2.84–2.77 (m, 12H), 1.70–1.68 (m, 12H), 1.42–1.28 (m, 48H), 0.90–0.86 (t, 18H). ^{13}C NMR (100 MHz, $CDCl_3$): δ 182.49, 154.53, 151.91, 141.07, 140.53, 140.37, 140.15, 139.06, 134.12, 133.14, 132.87, 132.44, 130.48, 130.10, 129.18, 115.18, 114.92, 31.90, 30.49, 30.27, 29.57, 29.50, 29.43, 29.31, 22.70, 14.14. MS (MALDI-TOF) *m*/*z*: calcd for $C_{82}H_{112}F_2O_2S_8$ $[M]^+$, 1422.64; found, 1422.53.

Compound DRCN6T-F. Under the protection of argon, compound DF8T-F (0.15 g, 0.145 mmol) and compound 5 (0.14 g, 0.72 mmol) were dissolved in a dry $CHCl_3$ (40 mL) solution, and then 0.03 mL piperidine was added to the mixture. After stirring and refluxing for 6 h, the reaction mixture was extracted with $CHCl_3$ (30 mL × 3), the organic layer was washed with water and dried over anhydrous Na_2SO_4 for 1 h. After removal of solvent, the crude product was purified by silica gel using chloroform as eluent. The crude product was recrystallized from $CHCl_3$ and hexane to give DRCN6T-F as a black solid (0.18 g, 87%).^{1}H NMR (400 MHz, $CDCl_3$): δ 7.98 (s, 2H), 7.29 (s, 2H), 7.18 (s, 2H), 6.96 (s, 2H), 4.34–4.29 (t, 4H), 2.85–2.80 (m, 8H), 1.72–1.65 (m, 8H), 1.44–1.28 (m, 16H), 0.90–0.87 (t, 12H); ^{13}C NMR (100 MHz, $CDCl_3$): δ 165.81,

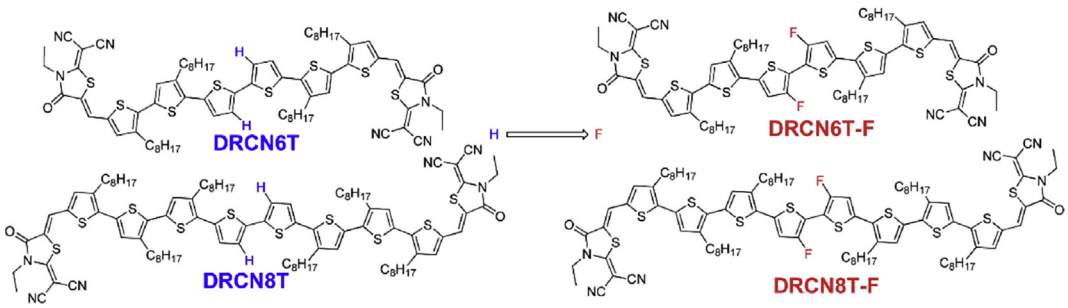

Scheme 1. The chemical structures of **DRCN6T** and **DRCN8T**, **DRCN6T-F** and **DRCN8T-F**.

165.49, 154.60, 151.97, 141.50, 141.42, 140.46, 138.78, 133.89, 133.05, 132.74, 132.03, 130.58, 128.41, 115.30, 115.04, 113.61, 113.30, 112.24, 55.63, 40.66, 31.87, 30.55, 30.14, 29.64, 29.56, 29.39, 29.32, 29.28, 22.68, 14.21, 14,12. MS (MALDI-TOF) *m/z*: calcd for $C_{74}H_{86}F_2N_6O_2S_8$ $[M]^+$, 1384.455; found, 1384.228. Anal. Calcd. For $C_{74}H_{86}F_2N_6O_2S_8$: C, 64.12; H, 6.25; N, 6.06. Found: C, 66.14; H, 6.42; N, 6.11.

Compound DRCN8T-F. Under the protection of argon, compound DF8T-F (0.15 g, 0.105 mmol) and compound 5 (0.10 g, 0.52 mmol) were dissolved in a dry $CHCl_3$ (50 mL) solution, and then 0.02 mL piperidine was added to the mixture. After stirring and refluxing for 6 h, the mixture was extracted with $CHCl_3$ (30 mL × 3), the organic layer was washed with water and dried over anhydrous Na_2SO_4 for 1 h. After removal of solvent, the crude product was purified by silica gel using chloroform as eluent. The crude product was recrystallized from $CHCl_3$ and hexane to give DRCN8T-F as a black solid (0.16 g, 86%). ^{1}H NMR (400 MHz, $CDCl_3$): δ 8.00 (s, 2H), 7.29 (s, 2H), 7.18 (s, 2H), 7.04 (s, 2H), 6.94 (s, 2H), 4.35–4.30 (t, 4H), 2.86–2.80 (m, 12H), 1.72–1.70 (m, 12H), 1.43–1.28 (m, 66H), 0.89–0.86 (t, 18H); ^{13}C NMR (100 MHz, $CDCl_3$): δ 164.53, 164.27, 139.91, 139.77, 139.67, 139.64, 137.60, 132.34, 131.48, 129.26, 129.24, 129.20, 128.89, 127.82, 127.28, 112.04, 111.98, 110.99, 54.15, 39.32, 30.56, 29.28, 29.20, 28.82, 28.36, 28.27, 28.22, 28.18, 28.10, 28.03, 27.99, 21.37, 12.90, 12.81. MS (MALDI-TOF) *m/z*: calcd for $C_{98}H_{122}F_2N_6O_2S_{10}$ $[M]^+$, 1774.703; found, 1774.928. Anal. Calcd. For $C_{98}H_{122}F_2N_6O_2S_{10}$: C, 66.32; H, 6.93; N, 4.74. Found: C, 66.41; H, 6.98; N, 4.83.

2.2. Instruments and characterization

The ^{1}H and ^{13}C NMR spectra were recorded on a Bruker AV400 Spectrometer. Matrix assisted laser desorption/ionization time-of-flight mass spectrometry (MALDI-TOF) were performed on a Bruker Autoflex III LRF200-CID instrument. The thermogravimetric analysis (TGA) and differential scanning calorimetry (DSC) were carried out on a NETZSCH STA 409PC instrument under purified nitrogen gas flow. The heating rate for TGA and DSC testing is 10 °C min^{-1}, and the cooling rate for DSC is 10 °C min^{-1}. UV–Vis spectra were obtained with a JASCO V-570 spectrophotometer. X-Ray diffraction (XRD) experiments were performed on a Rigaku D/max-2500 X-ray diffractometer with Cu-Kα radiation at a generator voltage of 40 kV and a current of 100 mA.

Cyclic voltammetry (CV) experiments were performed with a LK2010 electrochemical workstation. All CV measurements were carried out at room temperature with a conventional three-electrode configuration employing a glassy carbon electrode as the working electrode, a saturated calomel electrode (SCE) as the reference electrode, and a Pt wire as the counter electrode. Dichloromethane was distilled from calcium hydride under dry nitrogen immediately prior to use. Tetrabutylammonium phosphorus hexafluoride (Bu_4NPF_6, 0.1 M) in dry dichloromethane was used as the supporting electrolyte, and the scan rate was 100 mV s^{-1}. The highest occupied molecular orbital (HOMO) and lowest unoccupied molecular orbital (LUMO) energy levels were calculated from the onset oxidation potential and the onset reduction potential, using the equation $E_{HOMO} = -(4.80 + E^{ox}_{onset})$, $E_{LUMO} = -(4.80 + E^{re}_{onset})$.

The geometry structures of DRCN6T-F and DRCN8T-F were optimized by using DFT calculations (B3LYP/6-31G*), and the frequency analysis was followed to assure that the optimized structures were stable states. All calculations were carried out using *Gaussian 09*.

Atomic force microscopy (AFM) was performed using Multimode 8 atomic force microscope in tapping mode. The transmission electron microscopy (TEM) investigation was performed on Philips Technical G^2 F20 at 200 kV. The specimen for TEM measurement was prepared by spin casting the blend solution on ITO/PEDOT:PSS substrate, then floating the film on a water surface, and transferring to TEM grids. Photoluminescence characterization is carried out using a FluoroMax-P luminescence spectrometer using a xenon lamp as the source of excitation. The excitation wavelength is 460 nm.

Space charge limited current (SCLC) mobility was measured using a diode configuration of ITO/PEDOT:PSS/donor:$PC_{71}BM$/Au for hole mobility and glass/Al/donor:$PC_{71}BM$/Al for electron mobility and fitting the results to a space charge limited form, where SCLC equation is described by:

$$J = \frac{9\varepsilon_0\varepsilon_r\mu_0 V^2}{8L^3}\exp\left(0.89\beta\sqrt{\frac{V}{L}}\right)$$

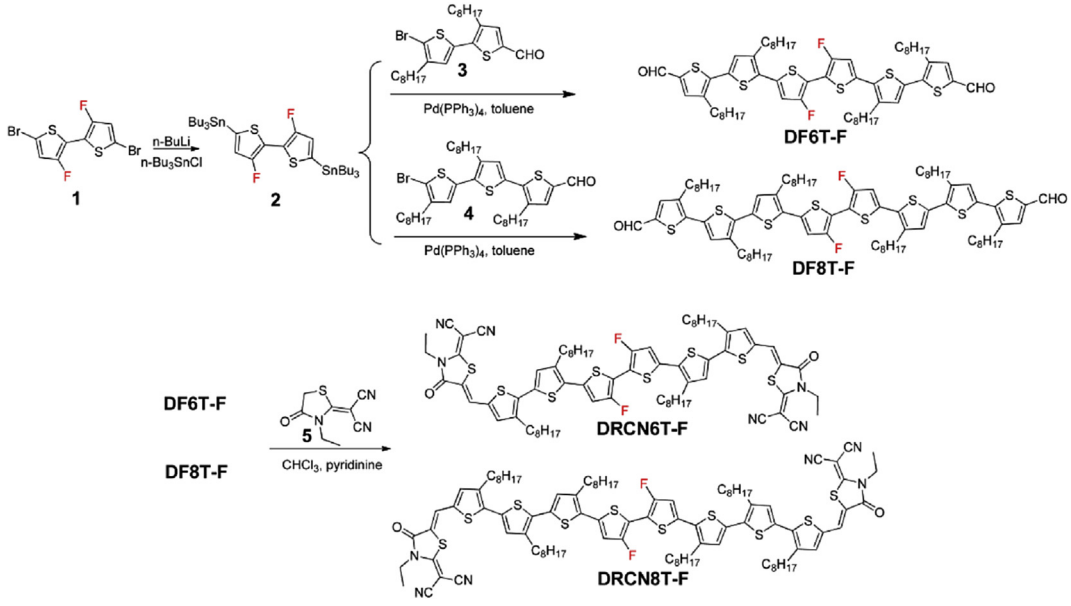

Scheme 2. The synthetic routes of molecules of DRCN6T-F and DRCN8T-F.

where J is the current density, L is the film thickness of the active layer, μ_0 is the mobility, ε_r is the relative dielectric constant of the transport medium, ε_0 is the permittivity of free space (8.85×10^{-12} F m^{-1}), V ($=V_{appl} - V_{bi}$) is the internal voltage in the device, where V_{appl} is the applied voltage to the device and V_{bi} is the built-in voltage due to the relative work function difference of the two electrodes.

2.3. Solar cell fabrication and testing

The devices were fabricated with a structure of glass/ITO/PEDOT:PSS/donor:$PC_{71}BM$/PFN-Br/Al. The ITO-coated glass substrates were cleaned by ultrasonic treatment in detergent, deionized water, acetone, and isopropyl alcohol under ultrasonication for 15 min each and subsequently dried by a nitrogen blow. A thin layer of PEDOT:PSS (Clevios P VP AI 4083, filtered at 0.45 μm) was spin-coated at 3000 rpm onto ITO surface. After baked at 150 °C for 20 min, the substrates were transferred into an argon-filled glove box. Subsequently, the active layer was spin-coated from blend chloroform solutions of donor and $PC_{71}BM$. For the devices based on DRCN6T-F, the substrates were then annealed at 100 °C for 10 min. For the devices based on DRCN8T-F, the substrates were then annealed at 110 °C for 10 min. Finally, a thin layer of PFN-Br (5 nm) from its methanol solution was spin-coated and 80 nm Al layer were deposited under high vacuum (<2×10^{-4} Pa). The effective areas of cells were 4 mm^2 defined by shadow masks. The current density-voltage (J-V) curves of photovoltaic devices were obtained by a Keithley 2400 source-measure unit. All masked and unmasked tests gave consistent results with relative errors within 5%. The photocurrent was measured under illumination simulated 100 mW cm^{-2} AM 1.5G irradiation using a SAN-EI XES-70S1solar simulator, calibrated with a standard Si solar cell. External quantum efficiencies were measured using Stanford Research Systems SR810 lock-in amplifier.

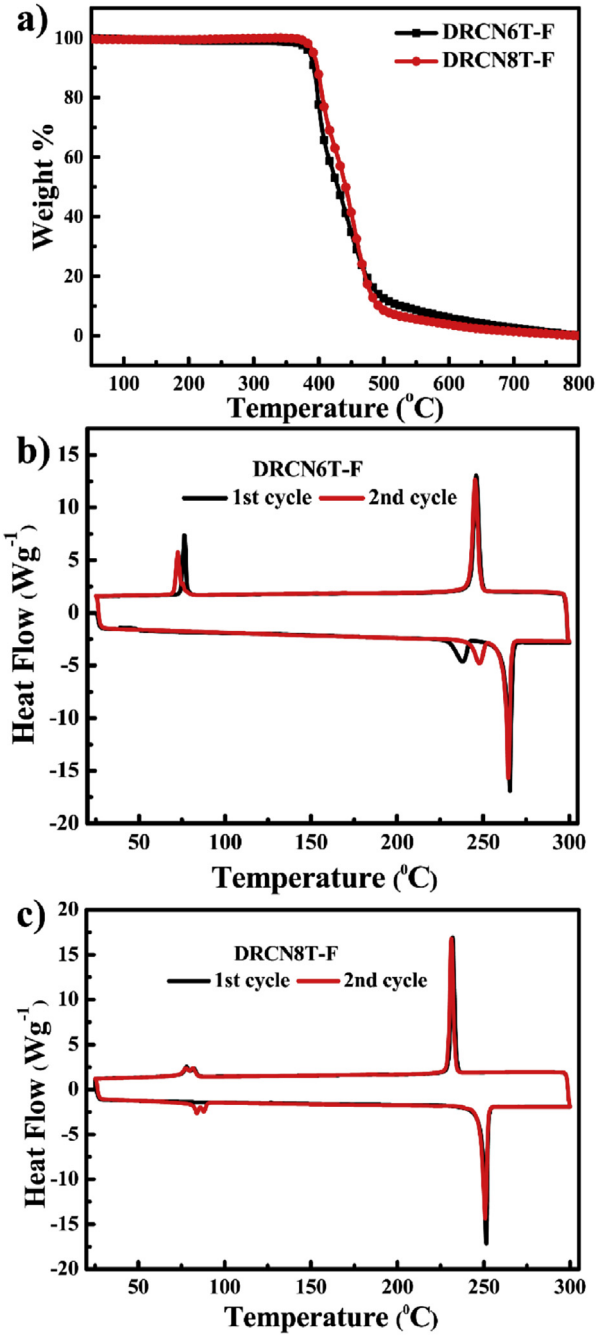

Fig. 1. a) TGA plot of **DRCN6T-F** and **DRCN8T-F**; b) DSC plots of **DRCN6T-F** with 2 cycles; c) DSC plots of **DRCN8T-F** with 2 cycles.

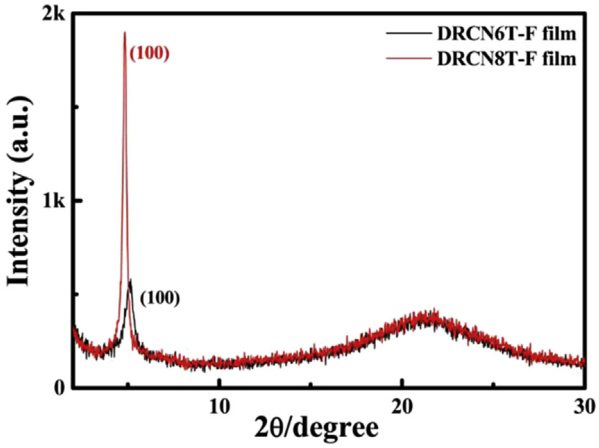

Fig. 2. XRD patterns of films **DRCN6T-F** and **DRCN8T-F** spin-coated from $CHCl_3$ onto glass substrate.

3. Results and discussion

3.1. Materials synthesis and characterization

The synthetic routes of **DRCN6T-F** and **DRCN8T-F** are illustrated in Scheme 2, and the detailed synthetic procedure and characterization data are presented in the Experimental section. The fluorinated intermediate compound 1 was synthesized according to the literature, and the tributylstannylation of compound 1 gave the ditin reagent 2 [40]. Compounds 3, 4 and 5 were synthesized based on our previous work [39,41]. The dialdehyde compounds DF6T-F and DF8T-F were then synthesized through Stille coupling reaction between compound 2 and 3 or 4 using $Pd(PPh_3)_4$ as catalyst, respectively. The targeted molecules, **DRCN6T-F** and **DRCN8T-F**, were synthesized via Knoevenagel condensation of the dialdehyde compounds with 2-(1,1-dicyanomethylene)-rhodanine in high yields. The chemical structure and purity of these two molecules were verified by ^{1}H and ^{13}C NMR, elemental analysis, and Time-off light (MALDI-TOF) MS. These two molecules exhibit good solubility in general organic solvents, such as chloroform, chlorobenzene, *etc*. Theoretical calculation results (Fig. S1), based on density functional

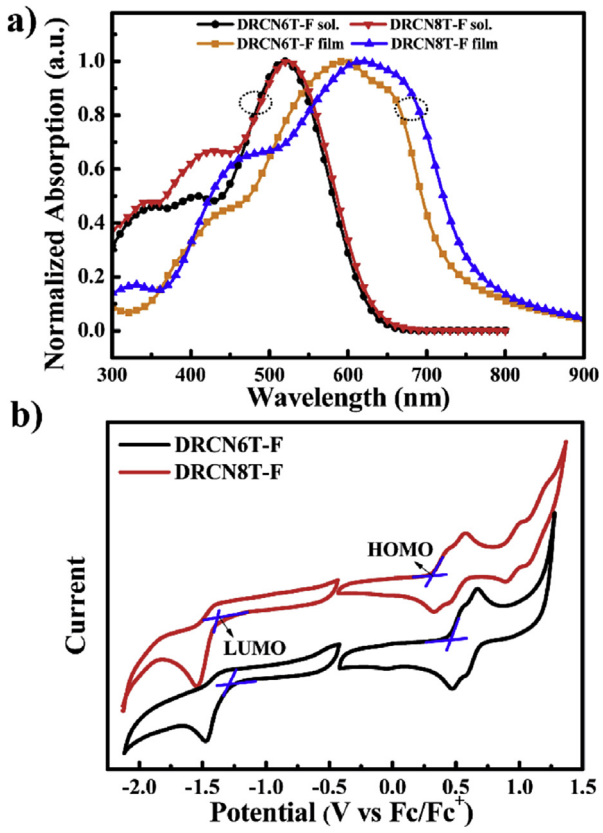

Fig. 3. a) UV–Vis absorption spectra of **DRCN6T-F** and **DRCN8T-F** in chloroform solutions and thin films; b) Cyclic voltammograms of **DRCN6T-F** and **DRCN8T-F** in dichloromethane solutions.

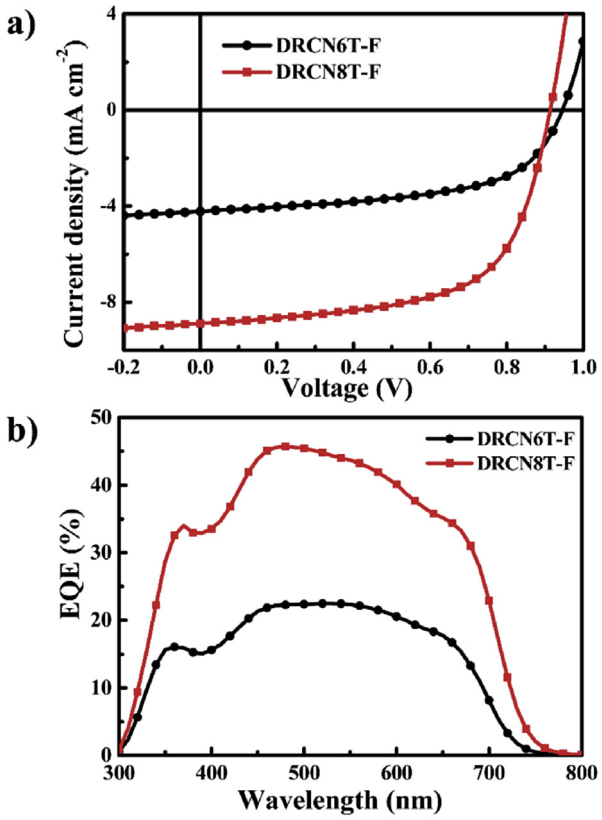

Fig. 4. a) Characteristic current density versus voltage (*J-V*) curves of the optimized devices based on **DRCN6T-F** and **DRCN8T-F** under simulated AM 1.5 G irradiation (100 mW cm^{-2}). b) The external quantum efficiency (EQE) curves of the optimized devices.

theory (DFT) at the B3LYP/6-31G(d) level, show that both molecules exhibit good coplanar conformations.

Thermogravimetric analysis (TGA) results suggest that both two molecules exhibit excellent thermal stability with decomposition temperatures (T_d) over 350 °C, which is necessary for the application in OPVs. Their solid state thermal transition were then determined by differential scanning calorimetry (DSC) analysis as shown in Fig. 1b and c. From their DSC plots, it can be seen that their second cycle are much similar to the first cycle. Obvious melting temperatures (T_m) and recrystallization (T_{cr}) points are obtained for both molecules, indicating the tendency to crystallize. In addition, their melting temperatures are over 40 °C higher than those for **DRCN6T** and **DRCN8T**, indicative an enhanced intermolecular interactions between these fluorinated small molecules due to the introduction of C–F bond [35,47].

The structural ordering of pristine **DRCN6T-F** and **DRCN8T-F** was investigated by X-ray diffraction (XRD) analysis for the films spin-coated from their $CHCl_3$ solutions onto glass substrates. As shown in Fig. 2, **DRCN6T-F** and **DRCN8T-F** exhibited a diffraction peak (100) at $2\theta = 5.2°$ and 4.8°, corresponding to a d_{100}-spacing value of 17.0 and 18.4 Å, respectively, which are smaller than those for their non-fluorinated molecules (18.5 Å for **DRCN6T** and 19.0 Å for **DRCN8T**).

3.2. Optical absorption and electrochemical properties

The UV–Vis absorption spectra of **DRCN6T-F** and **DRCN8T-F** in $CHCl_3$ solution and in thin film are shown in Fig. 3a, and the corresponding data are summarized in Table 1. Compared to their non-fluorinated counterparts (**DRCN6T** and **DRCN8T**), **DRCN6T-F** and

Table 2
The photovoltaic performance of **DRCN6T-F** and **DRCN8T-F** based devices.

Molecules	V_{oc} (V)	J_{sc} (mA cm^{-2})	J_{sc}^{EQE} (mA cm^{-2})	FF	PCE (%)
DRCN6T-F[a]	0.94	4.19	4.04	0.57	2.26
DRCN8T-F[b]	0.90	8.80	8.40	0.64	5.07
DRCN6T[c]	0.92	11.45	10.93	0.58	6.33
DRCN8T[c]	0.86	10.80	10.48	0.68	6.37

[a] With thermal annealing at 100 °C for 10 min.
[b] With thermal annealing at 110 °C for 10 min.
[c] Data are obtained from Ref. [6].

Table 1
Optical and electrochemical data of compounds **DRCN6T-F** and **DRCN8T-F**.

Molecules	λ_{max}^{sol} (nm)	λ_{max}^{film} (nm)	λ_{onset}^{film} (nm)	E_g^{opt} (eV)	$HOMO^{CV}$ (eV)	$LUMO^{CV}$ (eV)	$HOMO^{Cal}$ (eV)	$LUMO^{Cal}$ (eV)
DRCN6T-F	519	595	766	1.62	−5.24	−3.51	−5.14	−3.11
DRCN8T-F	524	619	780	1.59	−5.13	−3.45	−4.87	−3.02
DRCN6T[a]	532	577	775	1.60	−5.16	−3.56	−5.10	−3.06
DRCN8T[a]	531	602	771	1.61	−5.02	−3.45	−4.82	−2.99

[a] Data are obtained from Ref. [6].

Table 3
The mobilities of **DRCN6T-F** and **DRCN8T-F**, **DRCN6T** and **DRCN8T**.

Molecules	μ_h ($cm^2\ V^{-1}\ s^{-1}$)	μ_e ($cm^2\ V^{-1}\ s^{-1}$)
DRCN6T-F	$(1.44 \pm 0.12) \times 10^{-4}$	$(2.19 \pm 0.18) \times 10^{-5}$
DRCN8T-F	$(8.24 \pm 0.20) \times 10^{-5}$	$(1.90 \pm 0.15) \times 10^{-5}$
DRCN6T[a]	2.61×10^{-4}	6.68×10^{-5}
DRCN8T[a]	5.77×10^{-4}	3.48×10^{-4}

[a] Data are obtained from Ref. [6].

DRCN8T-F in solutions display a blue-shift of 13 and 7 nm at maximum absorption peak (λ_{max}), which are 519 and 524 nm, respectively. In their solid state, these two molecules exhibit an obvious red-shifted and broadened absorption (in range from 400 to 750 nm) compared to their solution absorption. The optical band gaps (E_g^{opt}) of **DRCN6T-F** and **DRCN8T-F** estimated from the onset of their film absorption are 1.62 and 1.59 eV, respectively, which are similar to those for the non-fluorinated analogues [6].

The molecular energy levels were measured by electrochemical cyclic voltammetry (CV) as shown in Fig. 3b. The highest occupied molecular orbital (HOMO) and lowest unoccupied molecular orbital (LUMO) energy levels, calculated from the onset oxidation and reduction potential, are −5.24 and −3.51 eV for **DRCN6T-F**, and −5.13 and −3.45 eV for **DRCN8T-F**, respectively. It can be seen that these two fluorinated small molecules both exhibit lower HOMO but similar LUMO energy levels compared to their non-fluorinated counterparts (Table 1), since the F atom weaken the electron-donating ability of 2,2′-bithiophene unit and the HOMO energies are largely dominated by the central donor unit in the A-D-A type small molecules [20]. These results are in good agreement with the trend of the calculation HOMO and LUMO results as summarized in Table 1. All above results demonstrated that the F atom attached on the 2,2′-bithiophene unit can tune the absorption as well as energy levels of the molecules.

3.3. Photovoltaic performance

Solution-processed BHJ devices were fabricated using these two fluorinated small molecules as the electron donor with a normal

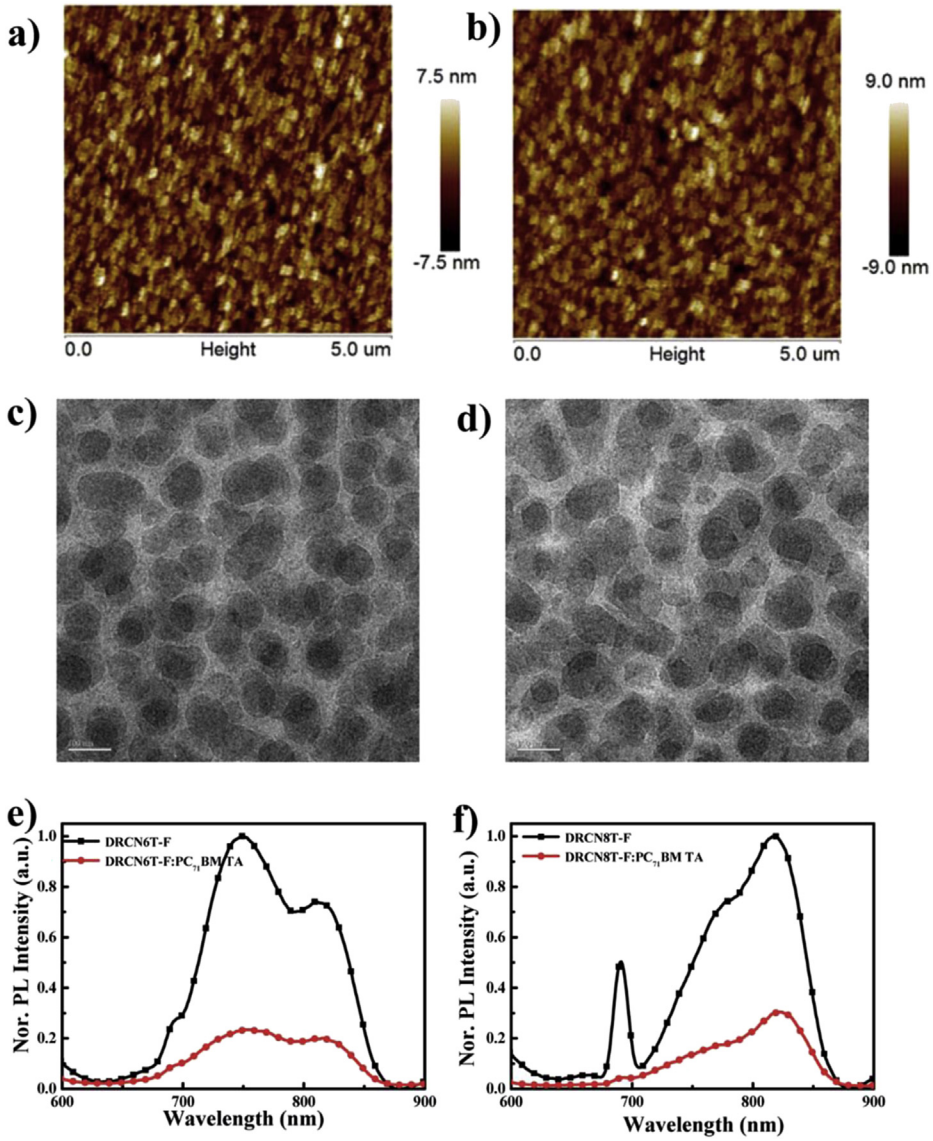

Fig. 5. Tapping-mode AFM height images of (a) **DRCN6T-F**:$PC_{71}BM$ blend films and (b) **DRCN8T-F**:$PC_{71}BM$ blend films, and TEM images of (c) **DRCN6T-F**:$PC_{71}BM$ blend films and (d) **DRCN8T-F**:$PC_{71}BM$ blend films. The scale bars are 100 nm. Photoluminescence (PL) spectra of (e) **DRCN6T-F** neat and blend films mixed with $PC_{71}BM$ with thermal annealing and (f) **DRCN8T-F** neat and blend films mixed with $PC_{71}BM$ with thermal annealing. The PL spectra was performed at an excitation wavelength of 460 nm.

device structure of ITO/PEDOT:PSS/Donor:$PC_{71}BM$/PFN-Br/Al, where PFN-Br is a widely used electron transport layer [48]. The optimized weight ratio of donor:$PC_{71}BM$ was 1:0.8 for these two small molecules. The *J*-V curves of the optimized devices were presented in Fig. 4a, and the corresponding photovoltaic parameters are summarized in Table 2. The optimized device performances were obtained with thermal annealing treatment. **DRCN6T-F** based devices exhibited a PCE of 2.26%, with a high open-circuit voltage (V_{oc}) of 0.94 V, but a low short-circuit current density (J_{sc}) of 4.19 mA cm^{-2} and fill factor (FF) of 0.57. The devices based on **DRCN8T-F** exhibited a PCE of 5.07%, with a V_{oc} of 0.90 V, a J_{sc} of 8.80 mA cm^{-2} and a moderate FF of 0.64. Compared with the **DRCN6T-F** based device, the device based on **DRCN8T-F** exhibits a lower series resistance (R_s) (8.4 vs. 22.8 Ω cm^2) and a higher shunt resistance (R_{sh}) (567 vs. 352 Ω cm^2), indicating a better ohmic contact in the **DRCN8T-F** based device and leading to its relatively high FF. For comparison, the photovoltaic parameters of **DRCN6T** and **DRCN8T** based devices are also listed in Table 2. It can be seen that these fluorinated small molecules based devices exhibit poorer performance than their non-fluorinated counterparts. Compared with the device parameters of **DRCN6T** and **DRCN8T**, higher V_{oc} values were achieved for **DRCN6T-F** and **DRCN8T-F** based devices, which is due to their lower HOMO energy levels. However, much lower J_{sc}, thus leading to lower PCEs, were obtained for **DRCN6T-F** and **DRCN8T-F** based devices due to the poor morphologies and low charge carrier mobilities as discussed below (see Table 3).

Their external quantum efficiency (EQE) were measured as shown in Fig. 4b, where the devices with **DRCN6T-F** and **DRCN8T-F** exhibit photo-to-current responses from 300 to 720 nm. It can be seen that the EQE for the DRCN8T-F based devices is higher than that of the **DRCN6T-F** based devices, which is in consistent with the trend of their blend films absorption results as depicted in Fig. S2. In addition, their EQE values are obviously lower than those for **DRCN6T** and **DRCN8T**. The calculated J_{sc} obtained from the EQE curves are 4.04 and 8.40 mA cm^{-2}, respectively, which show a reasonably mismatch compared with the J_{sc} values obtained from their *J*-*V* curves.

The active layer morphologies were measured by atomic force microscopy (AFM) and transmission electron microscopy (TEM). As shown in Fig. 5a and b, it is found that the films of **DRCN6T-F** and **DRCN8T-F** blended with $PC_{71}BM$ show a root-mean-square (rms) surface roughness of 2.00 and 2.21 nm, respectively. From their TEM images (Fig. 5c and d), large domain with sizes of ca. 80 nm, were observed in their blend films, which is much larger than the exciton diffusion length (ca. 10–20 nm), thus leading to serious charge recombination and then inferior J_{sc} values [49]. These black domains should be formed from the fullerene material, which means that the donor-acceptor compatibility decreases for these fluorinated molecules compared to the un-substituted counterparts. This might be driven by the strong intermolecular interactions between these fluorinated molecules [29,34,45]. The photoluminescence (PL) spectra of the pure **DRCN6T-F** and DRCN8T-F film and their blended films with TA treatment were measured and the results were shown in Fig. 5e and f. Low PL quenching efficiencies of 75% and 71% were observed for the **DRCN6T-F** and **DRCN8T-F** active layers, respectively, which suggested that significant extent of excitons are not able to diffuse at the donor-acceptor interfaces and that charge transfer events are not occurring effectively [49,50].

The mobilities of the optimized devices were measured by the space charge limited current (SCLC) method (Fig. S3). The hole and electron mobilities for **DRCN6T-F**-based devices are $(1.44 \pm 0.12) \times 10^{-4}$ and $(2.19 \pm 0.18) \times 10^{-5}$ cm^2 V^{-1} s^{-1}, respectively. For **DRCN8T-F** based devices, the hole and electron mobilities are $(8.24 \pm 0.20) \times 10^{-5}$ and $(1.90 \pm 0.15) \times 10^{-5}$ cm^2 V^{-1} s^{-1}, respectively. Their charge mobilities are obviously lower than those of the **DRCN6T** and **DRCN8T**. The low charge carrier mobilities are detrimental for charge transport and collection, thus leading their low J_{sc} values [50]. These results are consistent with their morphological results as discussed above.

4. Conclusion

In this work, we designed and synthesized two new fluorinated small molecules, **DRCN6T-F** and **DRCN8T-F**, with 3,3′-difluoro-2,2′-bithiophene as the central unit and 2-(1,1-dicyanomethylene)-rhodanine as the ending groups. Compared to their non-fluorinated counterparts **DRCN6T** and **DRCN8T, DRCN6T-F** and **DRCN8T-F** exhibit enhanced intermolecular interactions and lower HOMO energy levels. Regrettably, the device performance based on **DRCN6T-F** and **DRCN8T-F** are 2.26% and 5.07%, respectively, which are lower than those of their non-fluorinated counterparts owing to the decreased J_{sc}. It was found that unfavorable morphologies with large phase separation and lower charge carrier mobilities were responsible for the low J_{sc} and the PCEs of the devices. It is interesting that during the preparation of this paper, Peng et al. reported a similar A-D-A type small molecule using the same fluorinated central unit, which exhibited better performance than its non-fluorinated counterpart [51]. These results demonstrated that furtherly comprehensive investigations are still highly needed on the correlation between the fluorinated unit effect and the corresponding molecules based photovoltaic device performances.

Acknowledgments

The authors gratefully acknowledge the financial support from MoST (2014CB643502, 2016YFA0200200), NSFC (51373078, 51422304 and 91433101), PCSIRT (IRT1257) and Tianjin city (13RCGFGX01121).

Appendix A. Supplementary data

Supplementary data related to this article can be found at http://dx.doi.org/10.1016/j.orgel.2016.08.014.

References

[1] G. Yu, J. Gao, J.C. Hummelen, F. Wudl, A.J. Heeger, Science 270 (1995) 1789–1790.
[2] Y. Liu, J. Zhao, Z. Li, C. Mu, W. Ma, H. Hu, K. Jiang, H. Lin, H. Ade, H. Yan, Nat. Commun. 5 (2014) 5293.
[3] I. Etxebarria, J. Ajuria, R. Pacios, Org. Electron 19 (2015) 34–60.
[4] Z. He, B. Xiao, F. Liu, H. Wu, Y. Yang, S. Xiao, C. Wang, T.P. Russell, Y. Cao, Nat. Photonics 9 (2015) 174–179.
[5] W. Yu, L. Huang, D. Yang, P. Fu, L. Zhou, J. Zhang, C. Li, J. Mater. Chem. A 3 (2015) 10660–10665.
[6] B. Kan, M. Li, Q. Zhang, F. Liu, X. Wan, Y. Wang, W. Ni, G. Long, X. Yang, H. Feng, Y. Zuo, M. Zhang, F. Huang, Y. Cao, T.P. Russell, Y. Chen, J. Am. Chem. Soc. 137 (2015) 3886–3893.
[7] L. Lu, T. Zheng, Q. Wu, A.M. Schneider, D. Zhao, L. Yu, Chem. Rev. 115 (2015) 12666–12731.
[8] L. Dou, Y. Liu, Z. Hong, G. Li, Y. Yang, Chem. Rev. 115 (2015) 12633–12665.
[9] J.D. Chen, C. Cui, Y.Q. Li, L. Zhou, Q.D. Ou, C. Li, Y. Li, J.X. Tang, Adv. Mater. 27 (2015) 1035–1041.
[10] W. Zhao, D. Qian, S. Zhang, S. Li, O. Inganäs, F. Gao, J. Hou, Adv. Mater. (2016). http://dx.doi.org/10.1002/adma.201600281.
[11] C. Duan, K. Zhang, C. Zhong, F. Huang, Y. Cao, Chem. Soc. Rev. 42 (2013) 9071–9104.
[12] Z.-G. Zhang, Y. Li, Sci. China Chem. 58 (2014) 192–209.
[13] K. Sun, Z. Xiao, S. Lu, W. Zajaczkowski, W. Pisula, E. Hanssen, J.M. White, R.M. Williamson, J. Subbiah, J. Ouyang, A.B. Holmes, W.W. Wong, D.J. Jones, Nat. Commun. 6 (2015) 6013.
[14] K. Gao, L. Li, T. Lai, L. Xiao, Y. Huang, F. Huang, J. Peng, Y. Cao, F. Liu, T.P. Russell, R.A. Janssen, X. Peng, J. Am. Chem. Soc. 137 (2015) 7282–7285.
[15] Q. Zhang, X. Wan, F. Liu, B. Kan, M. Li, H. Feng, H. Zhang, T.P. Russell, Y. Chen, Adv. Mater. (2016). http://dx.doi.org/10.1002/adma.201601435.
[16] B. Qiu, J. Yuan, Y. Zou, D. He, H. Peng, Y. Li, Z. Zhang, Org. Electron 35 (2016)

87–94.
[17] J. Min, C. Cui, T. Heumueller, S. Fladischer, X. Cheng, E. Spiecker, Y. Li, C.J. Brabec, Adv. Energy Mater. (2016). http://dx.doi.org/10.1002/aenm.201600515.
[18] Y. Lin, F. Zhao, Q. He, L. Huo, Y. Wu, T.C. Parker, W. Ma, Y. Sun, C. Wang, D. Zhu, A.J. Heeger, S.R. Marde, X. Zhan, J. Am. Chem. Soc. 138 (2016) 4955–4961.
[19] A. Mishra, P. Bäuerle, Angew. Chem. Int. Ed. 51 (2012) 2020–2067.
[20] Y. Chen, X. Wan, G. Long, Acc. Chem. Res. 46 (2013) 2645.
[21] W. Ni, M. Li, X. Wan, Y. Zuo, B. Kan, H. Feng, Q. Zhang, Y. Chen, Sci. China Chem. 58 (2014) 339–346.
[22] J. Roncali, P. Leriche, P. Blanchard, Adv. Mater 26 (2014) 3821–3838.
[23] J.E. Coughlin, Z.B. Henson, G.C. Welch, G.C. Bazan, Acc. Chem. Res. 47 (2014) 257–270.
[24] L. Yuan, K. Lu, B. Xia, J. Zhang, Z. Wang, Z. Wang, D. Deng, J. Fang, L. Zhu, Z. Wei, Adv. Mater. (2016). http://dx.doi.org/10.1002/adma.201600512.
[25] Y.N. Luponosov, J. Min, A.N. Solodukhin, O.V. Kozlov, M.A. Obrezkova, S.M. Peregudova, T. Ameri, S.N. Chvalun, M.S. Pshenichnikov, C.J. Brabec, Org. Electron. 32 (2016) 157–168.
[26] K. Gao, J. Miao, L. Xiao, W. Deng, Y. Kan, T. Liang, C. Wang, F. Huang, J. Peng, Y. Cao, Adv. Mater. 28 (2016) 4727–4733.
[27] Y. Wang, Q. Zhang, F. Liu, X. Wan, B. Kan, H. Feng, X. Yang, T.P. Russell, Y. Chen, Org. Electron. 28 (2016) 263–268.
[28] A. Tang, C. Zhan, J. Yao, Chem. Mater. 27 (2015) 4719–4730.
[29] A.C. Stuart, J.R. Tumbleston, H. Zhou, W. Li, S. Liu, H. Ade, W. You, J. Am. Chem. Soc. 135 (2013) 1806–1815.
[30] Z. Mao, K. Vakhshouri, C. Jaye, D.A. Fischer, R. Fernando, D.M. DeLongchamp, E.D. Gomez, G. Sauvé, Macromolecules 46 (2013) 103–112.
[31] M. Zhang, X. Guo, S. Zhang, J. Hou, Adv. Mater. 26 (2014) 1118–1123.
[32] P. Liu, K. Zhang, F. Liu, Y. Jin, S. Liu, T.P. Russell, H.-L. Yip, F. Huang, Y. Cao, Chem. Mater. 26 (2014) 3009–3017.
[33] W. Li, S. Albrecht, L. Yang, S. Roland, J.R. Tumbleston, T. McAfee, L. Yan, M.A. Kelly, H. Ade, D. Neher, W. You, J. Am. Chem. Soc. 136 (2014) 15566–15576.
[34] J.W. Jung, J.W. Jo, C.C. Chueh, F. Liu, W.H. Jo, T.P. Russell, A.K. Jen, Adv. Mater. 27 (2015) 3310–3317.
[35] M.A. Uddin, T.H. Lee, S. Xu, S.Y. Park, T. Kim, S. Song, T.L. Nguyen, S.-J. Ko, S. Hwang, J.Y. Kim, H.Y. Woo, Chem. Mater. 27 (2015) 5997–6007.
[36] J. Zhao, Y. Li, G. Yang, K. Jiang, H. Lin, H. Ade, W. Ma, H. Yan, Nat. Energy 1 (2016) 15027.
[37] A.K. Kyaw, D.H. Wang, D. Wynands, J. Zhang, T.Q. Nguyen, G.C. Bazan, A.J. Heeger, Nano Lett. 13 (2013) 3796–3801.
[38] J.L. Wang, F. Xiao, J. Yan, Z. Wu, K.K. Liu, Z.F. Chang, R.B. Zhang, H. Chen, H.B. Wu, Y. Cao, Adv. Funct. Mater. 26 (2016) 1803–1812.
[39] J. Wang, K. Liu, J. Yan, Z. Wu, F. Liu, F. Xiao, Z. Chang, H. Wu, Y. Cao, T.P. Russell, J. Am. Chem. Soc. 138 (2016) 7687–7697.
[40] H.J. Son, W. Wang, T. Xu, Y. Liang, Y. Wu, G. Li, L. Yu, J. Am. Chem. Soc. 133 (2011) 1885–1894.
[41] B.C. Schroeder, Z. Huang, R.S. Ashraf, J. Smith, P. D'Angelo, S.E. Watkins, T.D. Anthopoulos, J.R. Durrant, I. McCulloch, Adv. Funct. Mater. 22 (2012) 1663–1670.
[42] H. Wang, X. Yu, C. Yi, H. Ren, C. Liu, Y. Yang, S. Xiao, J. Zheng, A. Karim, S.Z.D. Cheng, X. Gong, J. Phys. Chem. C 117 (2013) 4358–4363.
[43] G. He, X. Wan, Z. Li, Q. Zhang, G. Long, Y. Liu, Y. Hou, M. Zhang, Y. Chen, J. Mater. Chem. C 2 (2014) 1337–1345.
[44] Q. Zhang, B. Kan, F. Liu, G. Long, X. Wan, X. Chen, Y. Zuo, W. Ni, H. Zhang, M. Li, Z. Hu, F. Huang, Y. Cao, Z. Liang, M. Zhang, T.P. Russell, Y. Chen, Nat. Photonics 9 (2015) 35–41.
[45] J.W. Jo, J.W. Jung, H.-W. Wang, P. Kim, T.P. Russell, W.H. Jo, Chem. Mater. 26 (2014) 4214–4220.
[46] Y. Liu, J. Zhou, X. Wan, Y. Chen, Tetrahedron 65 (2009) 5209–5215.
[47] H.G. Kim, B. Kang, H. Ko, J. Lee, J. Shin, K. Cho, Chem. Mater. 27 (2015) 829–838.
[48] T. Yang, M. Wang, C. Duan, X. Hu, L. Huang, J. Peng, F. Huang, X. Gong, Energy Environ. Sci. 5 (2012) 8208–8214.
[49] C.M. Proctor, M. Kuik, T.-Q. Nguyen, Prog. Polym. Sci. 38 (2013) 1941–1960.
[50] P.W. Blom, V.D. Mihailetchi, L.J.A. Koster, D.E. Markov, Adv. Mater. 19 (2007) 1551–1566.
[51] Z. Wang, Z. Li, J. Liu, J. Mei, K. Li, Y. Li, Q. Peng, ACS Appl. Mater. Inter. 8 (2016) 11639–11648.